Wind and Structures, *Vol. 27, No. 1 (2018) 11-27*
DOI: https://doi.org/10.12989/was.2018.27.1.011

A study on the action mechanism of internal pressures in straight-cone steel cooling tower under two-way coupling between wind and rain

S.T. Ke[*1], L.Y. Du[1a], Y.J. Ge[2b], Q. Yang[1c], H. Wang[3d] and Y. Tamura[4e]

[1]*Department of Civil Engineering, Nanjing University of Aeronautics and Astronautics, 29 Yudao Road, Nanjing 210016, China*
[2]*State Key Laboratory for Disaster Reduction in Civil Engineering, Tongji University, 1239 Siping Road, Shanghai 200092, China*
[3]*School of Civil Engineering, Southeast University, 2 Sipailou Road, Nanjing 210096, China*
[4]*Center of Wind Engineering Research, Tokyo Polytechnic University, 1583 Iiyama, Atsugi, Kanagawa 243-0297, Japan*

(Received August 5, 2017, Revised January 27, 2018, Accepted February 27, 2018)

Abstract. The straight-cone steel cooling tower is a novel type of structure, which has a distinct aerodynamic distribution on the internal surface of the tower cylinder compared with conventional hyperbolic concrete cooling towers. Especially in the extreme weather conditions of strong wind and heavy rain, heavy rain also has a direct impact on aerodynamic force on the internal surface and changes the turbulence effect of pulsating wind, but existing studies mainly focus on the impact effect brought by wind-driven rain to structure surface. In addition, for the indirect air cooled cooling tower, different additional ventilation rate of shutters produces a considerable interference to air movement inside the tower and also to the action mechanism of loads. To solve the problem, a straight-cone steel cooling tower standing 189 m high and currently being constructed is taken as the research object in this study. The algorithm for two-way coupling between wind and rain is adopted. Simulation of wind field and raindrops is performed with continuous phase and discrete phase models, respectively, under the general principles of computational fluid dynamics (CFD). Firstly, the rule of influence of 9 combinations of wind sped and rainfall intensity on flow field mechanism, the volume of wind-driven rain, additional action force of raindrops and equivalent internal pressure coefficient of the tower cylinder is analyzed. On this basis, the internal pressures of the cooling tower under the most unfavorable working condition are compared between four ventilation rates of shutters (0%, 15%, 30% and 100%). The results show that the 3D effect of equivalent internal pressure coefficient is the most significant when considering two-way coupling between wind and rain. Additional load imposed by raindrops on the internal surface of the tower accounts for an extremely small proportion of total wind load, the maximum being only 0.245%. This occurs under the combination of 20 m/s wind velocity and 200 mm/h rainfall intensity. Ventilation rate of shutters not only changes the air movement inside the tower, but also affects the accumulated amount and distribution of raindrops on the internal surface.

Keywords: straight-cone; steel cooling tower; two-way coupling between wind and rain; ventilation rate of shutters; aerodynamic force on internal surface; action mechanism; parameter analysis

1. Introduction

Large straight-cone steel cooling tower is a novel type of cooling towers and usually made of unique materials. This type of cooling tower has different distribution of aerodynamic force and flow field characteristics on internal surface compared with reinforced concrete cooling tower (Ke *et al*. 2015). Under extreme weathers, structures are not only subject to the action of strong wind, but also to the attack of heavy rain. Trajectories of raindrops are usually oblique under the joint action of wind force and gravity. The internal wall of tower cylinder is impacted by high-velocity raindrops that enter the open top of the cooling tower. This leads to significant changes in distribution of aerodynamic forces on the internal surface of the tower. Moreover, heavy rain will change the turbulence effect of pulsating wind compared with the rainless weather condition. In addition, different ventilation rate of shutters around the tower cylinder also affects air movement inside the tower and causes great changes in the intensity and position of raindrop impact. Therefore, understanding the action mechanism of loads on the internal surface of large straight-cone steel cooling tower under different combinations of wind velocity and rainfall intensity is of high theoretical and application values.

Many numerical simulations and wind tunnel tests have been conducted to analyze the internal pressure distribution and action mechanism for large cooling towers under different ventilation rates of shutters (Ke *et al.* 2015), heights and latitudes (Goudarzi and Sabbagh-Yazdi 2011), multi-tower arrangements (Cheng *et al.* 2013), tower configuration profile (Du and Ke 2015) and internal components of tower cylinder (Dong *et al.* 2015). The research results provide guidance for determining the values of internal pressure and for wind-resistant design of conventional hyperbolic concrete cooling towers. But studies on the aerodynamic performance on the internal surface of straight-cone steel cooling tower are very few under different combinations of wind velocity and rainfall

*Corresponding author, Associate Professor
E-mail: keshitang@163.com
[a] Postgraduate, E-mail: dlynuaa@163.com
[b] Professor, E-mail: yaojunge@tongji.edu.cn
[c] Professor, E-mail: yangqing@czu.cn
[d] Professor, E-mail: wanghao1980@seu.edu.cn
[e] Professor, E-mail: yukio@arch.t-kougei.ac.jp

ISSN: 1226-6116 (Print), 1598-6225 (Online)

Table 1 Two classifications of rainfall intensity

Grade of rainfall intensity	Light rain	Moderate rain	Heavy rain	Rainstorm	Downpour			
					Weak	Moderate	Strong	Extreme
Daily (mm/24h)	10	25	50	100	200			
Hourly (mm/h)	2.5	8	16	32	64	100	200	709.2

intensity. There are even fewer studies on the influence of different ventilation rates of shutters on internal pressure of the cooling tower. Those concerning with the joint action of wind and rain (Blocken *et al*. 2010, Blocken and Carmeliet 2004, Xin *et al.* 2012, Bennett *et al.* 2011, Wang and Xu 2010, Fu *et al*. 2016, Zhang *et al.* 2010, Wang *et al.* 2013) mainly deal with low-rise buildings, long-span bridge, inclined cables, power transmission towers and wind turbines. However, the potential influence of wind-driven rain on the aerodynamic performance on the internal surface of large cooling towers is much less reported.

We study a straight-cone steel cooling tower standing 189 m high and currently being constructed. Wind field around the cooling tower is simulated numerically under different wind velocities using CFD tools. Discrete phase model (DPM) is introduced into the stable wind field so as to input different rainfall intensities. Two-way coupling between wind and rain is realized by simultaneous iteration of raindrops and wind field. The action mechanism of internal pressure on tower cylinder is analyzed under the joint action of wind and rain. Then the rule of influence of wind velocity and rainfall intensity on the volume of wind-driven rain, additional load imposed by raindrops and equivalent internal pressure is extracted. Finally the representative values of equivalent internal pressure coefficient are provided for different segments of the tower under different ventilation rates of shutters.

2. Two-way coupling between wind and rain

2.1 Rainfall intensity

Rainfall intensity (R) is defined as flux of rainfall passing through a horizontal plane in unit time, usually in the unit of mm/h. Compared with mean precipitation in 12h and 24h used in meteorology, hourly precipitation is a more intuitive measure of the influence of instantaneous rainfall intensity during extreme weather events on structure performance. Therefore, hourly precipitation is a meaningful indicator in the engineering field. Table 1 shows two classification of rainfall intensity based on different sampling time. It can be seen from the table that the measurements of the same rainfall event differ greatly under different classifications. Here hourly rainfall intensity is used.

2.2 Raindrop size spectrum

Raindrops are usually considered as spheres, and raindrop size distribution is characterized using approximate diameter of the raindrops. Raindrop size distribution varies with time and space, and raindrop size function is known as raindrop size distribution, which approximately obeys a negative exponential distribution. The commonly used models to describe raindrop size distribution (Mcfarquhar and List 2010) include Best's size distribution, Marshall-Palmer distribution and Gamma raindrop size distribution. We adopt Marshall-Palmer distribution, as expressed in formula (1)

$$n(D) = N_0 e^{-\lambda D} \tag{1}$$

where D is the raindrop diameter, in the unit of mm; $n(D)$ is the raindrop number concentration spectrum of raindrops of different diameters; N_0 is the raindrop number concentration, usually taken as a constant equivalent to 8000; λ is the scale parameter, given by formula (2)

$$\lambda = 4.1 \times R^{-0.21} \tag{2}$$

2.3 Terminal velocity of raindrops

The descending velocity of raindrops increases continuously under the action of gravitation and the air resistances increases as well. Raindrops finally fall at a uniform velocity, which is the terminal velocity of raindrops. According to J.O. Lows (Gunn and Kinzer 2010), all raindrops will reach the terminal velocity after a fall distance≥20m.

In Marshall and Palmer (1948), Rigby *et al.* (2010), raindrops smaller than 2 mm are considered as spheres as they fall. However, air resistance will induce large deformation of raindrops over 2 mm in diameter. The following empirical formula is proposed to estimate the terminal velocity of raindrops in the vertical direction (formula (3))

$$v(D) = 9.1549\left(\frac{D}{2}\right)^{0.5} - 2.6549 + 2.5342e^{-3.727\left(\frac{D}{2}\right)^{0.5}} - 0.389\left(\frac{D}{2}\right)^{2.18} \tag{3}$$

where $v(D)$ is terminal velocity of raindrop with a diameter of D in the vertical direction (m/s).

2.4 Solving the two-way coupling between wind and rain

During the downpour, the volume fraction of raindrops in air is far smaller than 10% (Liu *et al.* 2002, Douvi and Margaris 2012). Here DMP model is used for raindrop simulation. It is the second phase integrated into the

continuous phase after the wind field stabilizes for solving two-way coupling between wind and rain. The dynamic equilibrium equation of motion of raindrops in a wind field is expressed as follows

$$\frac{d\vec{u}_p}{dt} = F_D(\vec{u} - \vec{u}_p) + \frac{\vec{g}(\rho_p - \rho)}{\rho_p} + \vec{F} \tag{4}$$

where $\vec{u}_p$ is the velocity of discrete phase (particle); $\vec{u}$ is the velocity of continuous phase (fluid); $F_D(\vec{u}-\vec{u}_p)$ is the drag force related to the mass of a unit particle; ρ_p and ρ are the densities of particle and fluid, respectively; $\vec{F}$ is the interaction force between the discrete phase and continuous phase, where

$$F_D = \frac{18\mu}{\rho_p d_p^2}\frac{C_D R_e}{24} \tag{5}$$

where μ is the coefficient of viscosity for the fluid; d_p is the particle diameter; *Re* is the relative Reynolds number, given by

$$Re = \frac{\rho d_p \left| u_p - u \right|}{\mu} \tag{6}$$

Considering the influence of raindrops as the discrete phase, the basic governing equation for wind as the continuous phase is expressed as

$$\frac{\partial \rho}{\partial t} + \nabla \cdot (\rho \vec{u}) = S_m \tag{7}$$

$$\frac{\partial}{\partial t}(\rho\vec{u}) + \nabla \cdot (\rho\vec{u}\vec{u}) = -\nabla p + \nabla \cdot (\bar{\tau}) + \rho\vec{g} + \vec{F} \tag{8}$$

where S_m is the mass of the second discrete phase after integrating the continuous phase; p is the pressure; $\bar{\tau}$ is the stress tensor; $\rho\vec{g}$ is gravity, and its stress tensor is given by

$$\bar{\tau} = \mu[(\nabla\vec{u} + \nabla\vec{u}^T) - \frac{2}{3}]\nabla\vec{u}I \tag{9}$$

where I is unit tensor. The second term on the right side of the equation represents volumetric expansion.

2.5 Particle-wall collision equation

The impact of raindrops on the wall surface of tower cylinder obeys the law of conservation of momentum. The key to solving the impact force lies in solving the time of collision. Evaporation, splash and rupture of raindrops during impact are neglected. The interaction between the raindrops and structure obeys Newton's second law of motion. In the momentum theorem

$$\int_0^\tau f(t)dt + \int_{v_s}^0 mdv = 0 \tag{10}$$

where $f(t)$ is the vector of impact force of a single raindrop, in the unit of N; v is the raindrop velocity.

The impact force imposed by the raindrop within unit time $F(\tau)$ is given by

$$F(\tau) = \frac{1}{\tau}\int_0^\tau f(t)dt = \frac{mv_s}{\tau} \tag{11}$$

The falling raindrops are considered as spheres

$$F(\tau) = \frac{mv_s}{\tau} = \frac{1}{6\tau}\rho\pi d_p^3 v_s \tag{12}$$

Raindrop diameter is generally below 6 mm, and the terminal velocity of raindrop is usually large before the impact. Therefore, to simplify the calculation, the time of collision τ is given by

$$\tau = \frac{d_p}{2v_s} \tag{13}$$

The impact force imposed by the raindrop to the structure is simplified as

$$F(\tau) = \frac{1}{6\tau}\rho\pi d_p^3 v_s = \frac{2v_s}{6d_p}\rho\pi d_p^3 v_s = \frac{1}{3}\rho\pi d_p^2 v_s^2 \tag{14}$$

3. An overview of the project and configuration of working conditions

3.1 An overview of the project

The super-large straight-cone steel cooling tower under construction stands 189 m. The height of air inlet is 32.5 m and the diameter is 144.5 m. The tower is built with steel frame support, which consists of main barrel, stiffening truss and accessory truss. The main barrel has 18 layers, and there are five layers of reinforcing truss, which are set up at the height of 32.5 m, 67 m, 107 m, 148 m and 189 m, respectively. The main barrel and reinforcing truss are made of Q345 steel. Accessory truss has 30 beams, which are made of Q235B steel. The structure above the height of air inlet is covered by windshield steel plates, which have regular and smooth surface. The base of the tower cylinder is equipped with shutters to regulate air intake. The structural specification is shown in Table 2.

3.2 Different combinations of wind and rain parameters

The tower is located in type B terrain. The aerodynamic performance on the internal surface of the cooling tower is compared under three combinations of wind velocity and rainfall intensity. Small wind, moderate wind and strong wind are defined based on the maximum wind velocity with a return period of 10, 50 and 100 years, respectively. Rainfall intensity is simulated as that of rain storm, and three levels of rainfall intensity are considered: weak, moderate and strong rain storms. Thus 9 combinations are calculated, as shown in Fig. 1.

Table 2 Structural specification of the large steel cooling tower

Design parameter	Value/m	Overall schematic
Tower top elevation	189	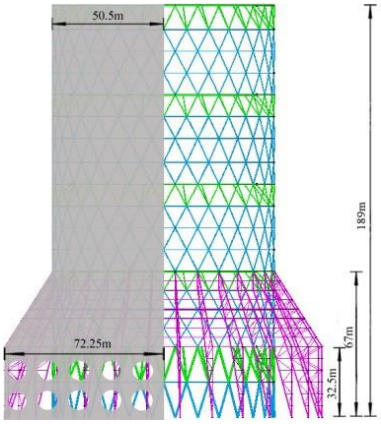
Inner diameter of air outlet	85	
Diameter of air outlet	101	
Top elevation of conical section	67	
Height of air inlet	32.5	
Diameter of air inlet	144.5	
Bottom diameter	144.5	

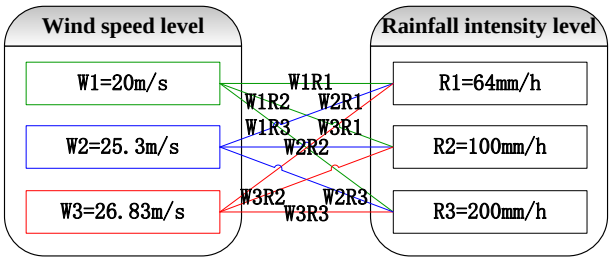

Fig. 1 Different combinations of wind and rain parameters

4. Numerical simulation through two-way coupling between wind and rain

4.1 Building a wind-rain field model

The entire computational domain has an along-wind length of 3000 m, an across-wind width of 1500 m, and a height of 600 m. The computational domain is divided into local and peripheral wind-rain fields during meshing. The local wind-rain field consists of the cooling tower model, and it is divided using non-structured meshes. The peripheral wind-rain field has a more regular shape and divided using structured meshes. The total mesh number is 16 million. Fig. 2 shows the schematic of the entire computational domain and meshing of the model.

The inlet of the computational domain is set as velocity inlet, and the outlet as pressure outlet. The two side walls are and top surface are symmetry boundaries. The tower and ground are set as walls. The overlap surfaces between the local and peripheral computational domains are interfaces. The computational domain of wind-rain field and its boundary conditions are shown in Fig. 3.

4.2 Wind-rain field coupling

The application of two-way coupling between wind and rain and discrete phase trajectory tracking to such structures with extra high Reynolds number raises a very high requirement on computer memory. Here, numerical calculation is undertaken by our large calculation server at the high-performance calculation center for aerodynamic design of wind turbines. Intel(R) Xeon(R) CPU E5-2650 v3 @ 2.30GHz is used (2 CPUs). The core number of CPU is 10 and the clock speed is 2.3 GHz. The memory installed is as high as 256GB, and 64-bit operating system is used.

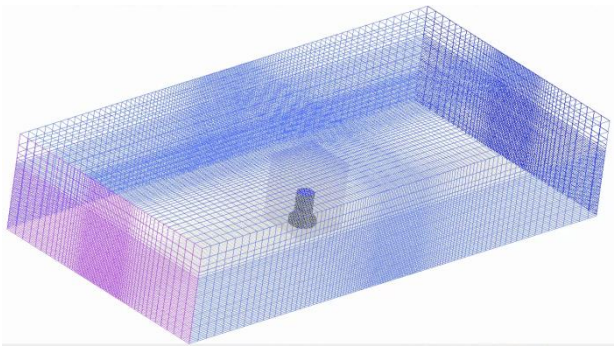

(a) Overall meshing

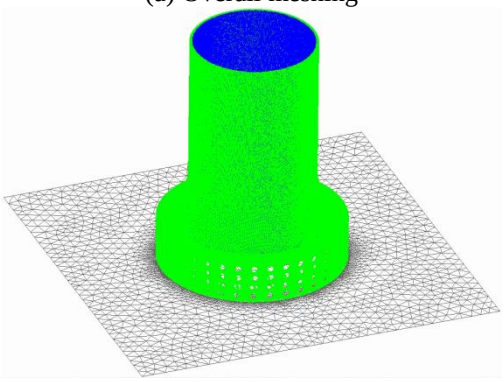

(b) Local meshing

Fig. 2 Schematic of overall and local meshing

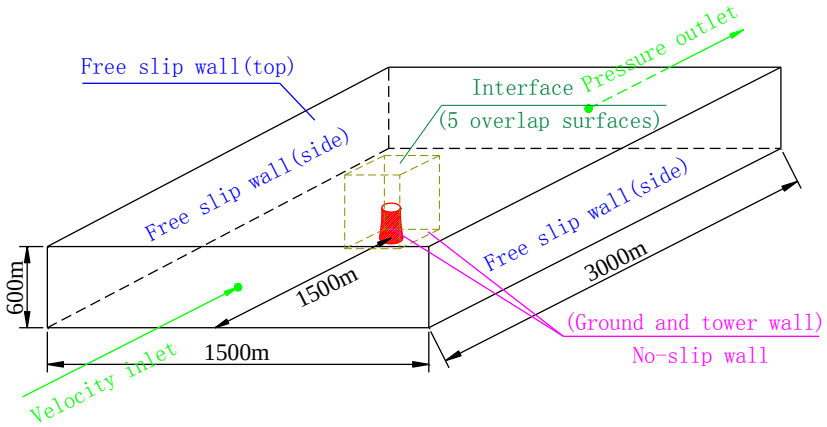

Fig. 3 Schematic of computational domain and boundary conditions

3D single-precision, segregated, standard finite volume solver is used. The flow field velocity is the absolute velocity. Air model is equivalent to ideal incompressible fluid, and the convection term is discretized into second-order upwind scheme. The k-ω shear-stress transport (SST) model is used as the computational model, and the energy switch is open. Default values of parameters are taken. The wind profile model with a power exponent of 0.15 is used for the inlet of the computational domain. The wind velocities at the height of 10m above the ground are set as three baseline wind velocities in section 2.2. The flow field is solved by the coupling between wind velocity and pressure via the SIMPLEC algorithm. In the calculation process, the grid tilt correction is set up to improve the calculation effect of the hybrid grid. The residual error of the control equation is set to 1×10^{-6}. The model of (enhanced) wall function is used in the simulation, and the law of logarithmic distribution of the underlying grid can be guaranteed. Then the wind field is initialized and iterative computation proceeds.

Fig. 4 shows the comparison of simulated, theoretical and measured values of mean wind velocity and turbulence intensity profile. The simulated mean wind velocity and turbulence intensity profiles agree well with the theoretical values, and the simulated values lie between the two measured values.

After the solution of wind field stabilizes, discrete phase is integrated for iterative computation of wind-rain field coupling. The number of raindrops in the along-wind and across-wind directions of the release surface is calculated by

$$0.01IXY\rho = \frac{4}{3}\pi(\frac{\bar{D}}{2})^3\rho AB \tag{15}$$

$$\frac{X}{Y} = \frac{A}{B} \tag{16}$$

Where I is the rainfall intensity; X and Y are respectively the along-wind length and across-wind width; ρ is the density of raindrop; $\bar{D}$ is the average particle diameter of raindrops; A and B are respectively the number of released raindrops in the along-wind and across-wind directions of the release surface.

Six raindrop diameters within the range of 1.0-6.0 mm are used to simulate precipitation with continuous distribution of raindrop diameter (Table 3). The occupancy of number and volume of raindrops with varying diameters is determined from the Marshall-Palmer distribution described in section 1.2. Then raindrops are released on a plane coincided with the top surface of the computing domain, with a horizontal velocity of 0. Under the action of wind force, raindrops finally achieve a velocity comparable to the horizontal wind velocity at the same position. The release velocity in the vertical direction is -5 m/s, downwards. The raindrops will reach the terminal velocity calculated in formula (3) under the joint action of gravity and resistance after falling for a sufficiently large distance.

The inner surface boundary condition of the cooling tower is set to capture (trap). In the coupling calculation of wind and rain, the number of rain drops can be displayed intelligently on the inner surface. The boundary of outer surface of the structure and other walls are set to escape (escape). When the raindrop meets the boundary, it stops the orbit calculation and records the basic information of the impact moment.

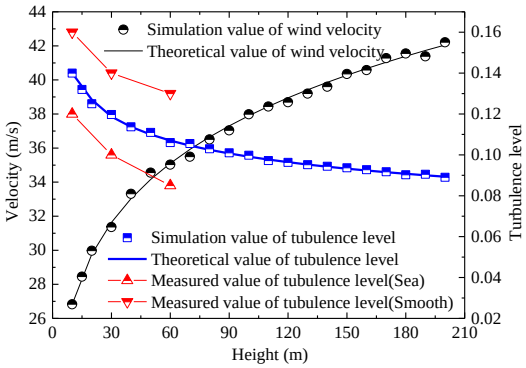

Fig. 4 Comparison of simulated wind velocity and turbulence intensity profile with the theoretical and measured value

Table 3 Different raindrop diameters

Raindrop diameter (mm)	1	2	3	4	5	6
Control range (mm)	0~1.5	1.5~2.5	2.5~3.5	3.5~4.5	4.5~5.5	5.5~6

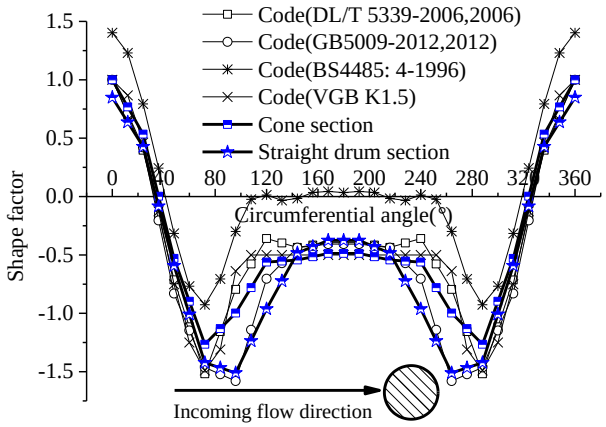

Fig. 5 Schematic of simulated wind pressure curves on the external surface of the tower and values in domestic and foreign standards

After the iteration is over, the result of continuous phase flow field and the raindrop data captured on the internal surface of the cooling tower are output. The impact of raindrops on the internal surface of the cooling tower is calculated, and the distribution pattern of equivalent internal pressure coefficient under the joint action of wind and rain is discussed.

4.3 Validation

The mean wind pressure coefficients of the conical and straight sections of the cooling tower are compared with the values of relevant codes (DL/T 5339-2006, 2006, VGB K1.5, GB50009-2012, 2012, BS4485: 4-1996), as shown in Fig. 5. It can be seen that the angles corresponding to the extreme values of negative wind pressure and separation points in the conical section are consistent with the values for smooth hyperbolic cooling tower for explosives in Chinese standard and also with the VGBK1.5 curve in German standard. The distribution curve of wind pressure coefficient in the straight section also agrees with the curves in Chinese load standard for structures with circular cross section. The wind pressure coefficients are larger according to UK standard, and they deviate greatly from other curves. Taken together, the result of numerical simulation in this paper is considered value.

5. Analysis under different combinations of wind and rain parameters

5.1 Wind field analysis

Figs. 6 and 7 are the vorticity contours and 3D wind velocity streamlines under the three baseline wind velocity v_0 before integrating the raindrops, respectively.

(1) The intensity of turbulence kinetic energy increases with the increase of wind velocity, with the peak occurring in the leeward region of shutters, air outlet and windward region of shutters under the maximum baseline wind velocity. The increment of turbulence kinetic energy decreases in the leeward region in the conical section, and it is larger under higher wind velocity than under low and moderate wind velocities.

(2) Part of the airflow goes inside the tower cylinder through the shutters, and moves along the internal surface of the tower, colliding with the internal surface and spiraling upwards. The radius decreases at the junction between the conical and straight sections, which hinders the upward movement of the airflow. This leads to an intact 3D airflow vortex and a significant increase in the pressure coefficient on the internal surface.

(3) As the wind velocity increases, the airflow moves at an accelerating speed along the tower cylinder, and the phenomenon of vortex shedding becomes more prominent. The wind velocity streamlines are more densely distributed, and the peak airflow velocities occurred in the lower shutters and air outlet at the top.

5.2 Rain field analysis

Raindrop trajectories are tracked based on the resultant velocity of particles. Fig. 8 is the schematic of raindrop trajectories in the coupled wind and rain fields under 9 working conditions. The level of raindrop density is subject to proportional coarsening. The following is observed from Fig. 8:

(1) Raindrops fall obliquely rather than vertically due to the action of wind. The inclination of raindrop trajectories becomes greater with the increase of wind velocity, but it is weakly affected by rainfall intensity.

(2) Raindrops go inside the cooling tower through the air outlet above and in front of the tower under the joint action of wind force, gravity and air resistance. They impact the leeward region in the middle and upper part of the internal surface at a high speed. The larger the rainfall intensity, the greater the number of raindrops accumulating on the internal wall surface.

(3) As wind velocity increases, there will be a significant increase in the horizontal force acting on the raindrops, which propels the along-wind movement of raindrops. A large number of raindrops slide over the tower top and move towards the back of the tower. This causes a dramatic reduction in the number of raindrops going inside the tower.

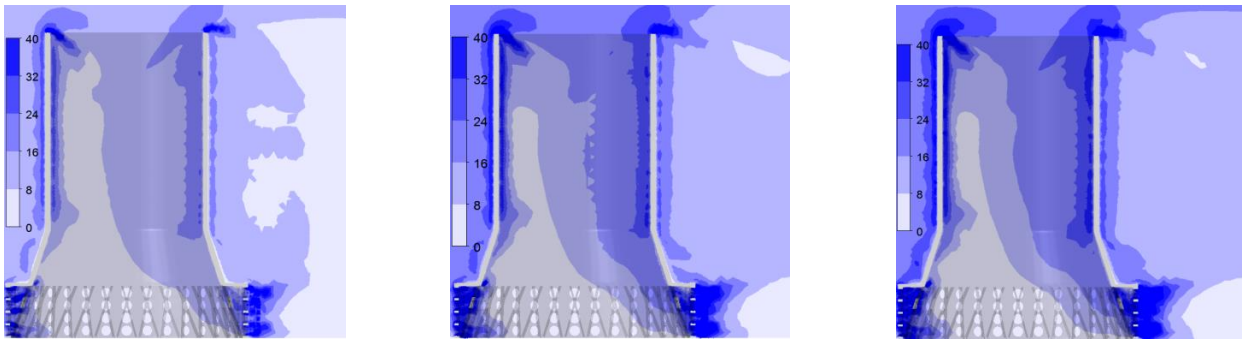

(a) v0=20 m/s (b) v0=25.3 m/s (c) v0=26.83 m/s

Fig. 6 Turbulence kinetic energy of the cooling tower under different wind velocities

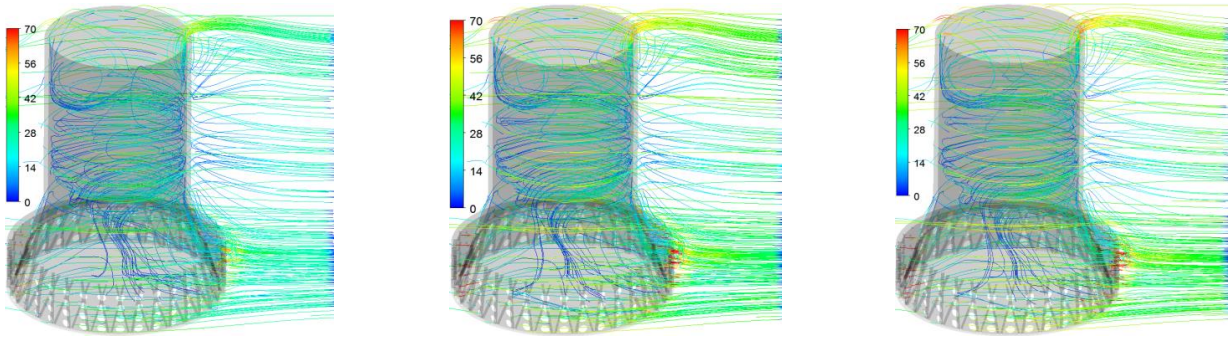

(a) v0=20 m/s (b) v0=25.3 m/s (c) v0=26.83 m/s

Fig. 7 3D wind velocity streamlines under different wind velocities

Fig. 9 shows the 3D distribution of raindrops on the internal surface of the cooling tower under different working conditions. To give a more clear visualization of positions impacted by raindrops, the coordinate system of the coupled wind and rain fields is rotated counterclockwise by 90°and the raindrops are coarsened. It can be seen from the figure that the leeward region in the upper part of the internal surface is most frequently impacted by raindrops under 9 working conditions. A few raindrops adhere to the windward region of the wall surface under the driving by airflow vortex inside the tower. The largest number of raindrops is collected on the internal surface under working condition W1R3. The number of collected raindrops decreases rapidly as the wind velocity increases, and it increases under larger rainfall intensity. This variation is more significant under lower wind velocity.

Airflow movement changes suddenly near the wall surface due to structural barrier and air outlet effect. However, the change of horizontal velocity of raindrops lags behind as compared with the change of wind velocity due to inertial effect. Therefore, the instantaneous velocity of raindrops impacting the wall surface is no longer equivalent to horizontal wind velocity. Fig. 10 shows the comparison of number, impact velocity and occupancy of velocity of raindrops with different diameters under 9 working conditions.

(1) Raindrop diameter varies from 3 to 6mm under different working conditions, and raindrops with a diameter of 5mm account for the largest proportion. This is because the velocity of smaller raindrops increases more rapidly under the same level of wind force. Smaller raindrops already slide over the tower top and go into the wake region instead of going inside the tower in the vertical direction.

(2) The largest number of collected raindrops occurs under working condition W1R3, followed by working condition W1R2 and W1R1 successively. A smaller number of raindrops are collected under other working conditions. The higher the wind velocity, the smaller the range of raindrop diameter; however, the later is directly proportional to rainfall intensity.

(3) The velocity of raindrops impacting the internal surface varies from 3 to 12 m/s. The occupancy of impact velocity of 3m/s is the highest under the working condition W1R1, W1R3 and W3R1; the occupancy of impact velocity of 6m/s is the highest under the working condition W1R2, W2R2, W2R3 and W3R3; the occupancy of impact velocity of 8 m/s is the highest under the working condition 4 and 8.

(4) The mean horizontal velocity of raindrops with varying diameter is far smaller than the minimum baseline wind velocity (20 m/s). The impact velocity generally decreases with the increase in raindrop diameter. The terminal velocity of raindrops under the working condition W3R2 is larger compared with other working conditions.

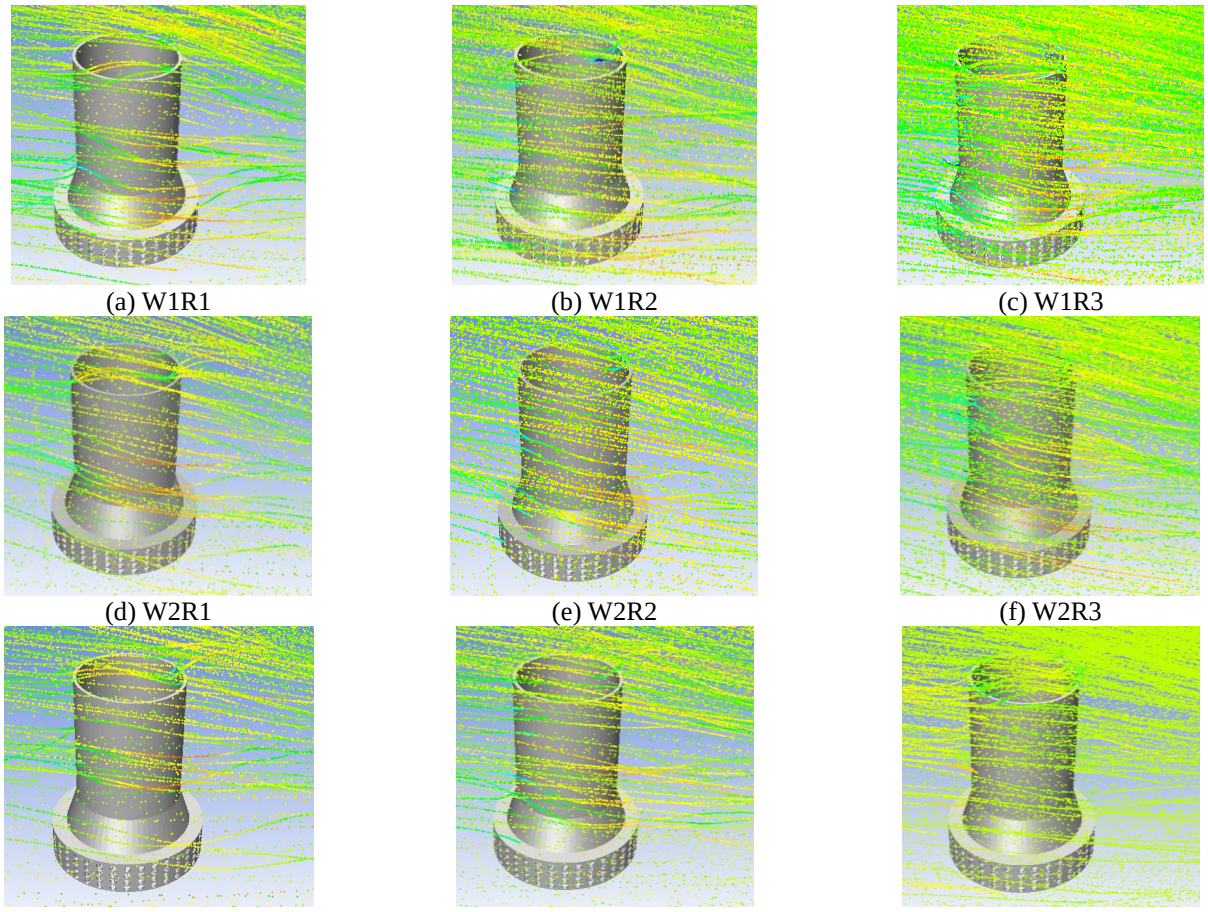

(a) W1R1 (b) W1R2 (c) W1R3

(d) W2R1 (e) W2R2 (f) W2R3

(g) W3R1 (h) W3R2 (i) W3R3

Fig. 8 Raindrop trajectories in the coupled wind and rain fields

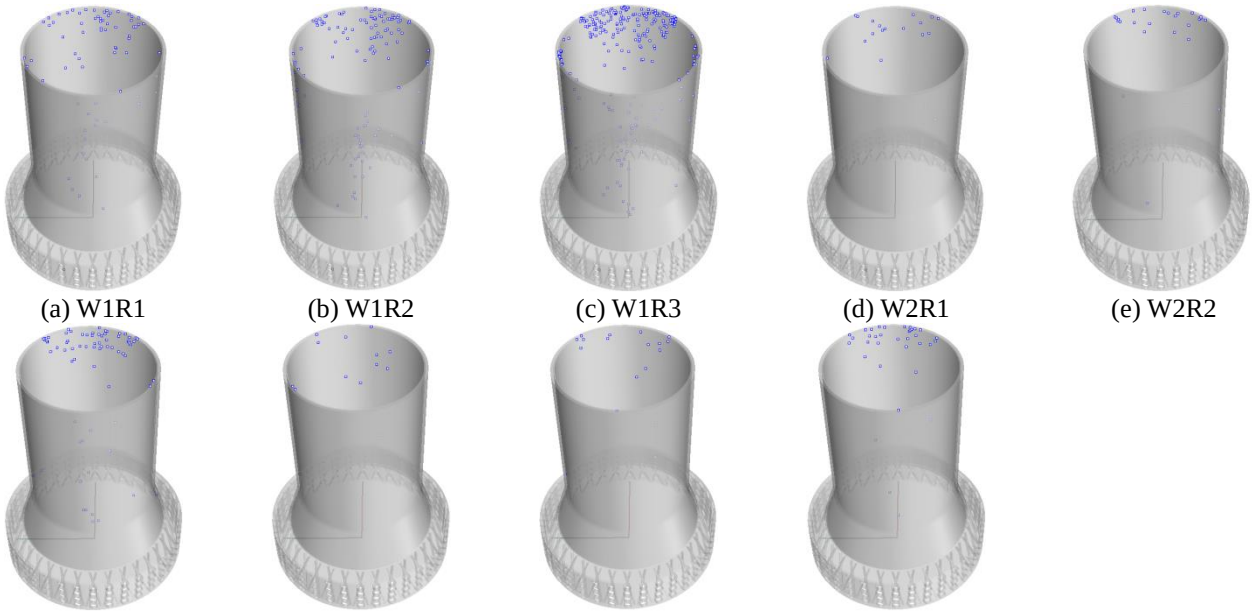

(a) W1R1 (b) W1R2 (c) W1R3 (d) W2R1 (e) W2R2

(f) W2R (g) W3R1 (h) W3R2 (i) W3R3

Fig. 9 3D distribution of raindrops on the internal surface of the cooling tower

Table 4 Comparison of wind and rain loads on the internal surface under different working conditions

Working condition	Total rain load (kN)	Total wind load (kN)	Total wind and rain load (kN)	Ratio (%)
W1R1	12.8	-16837	-16824	0.0761
W1R2	16.98	-16724	-16707	0.1016
W1R3	40.93	-16744	-16703	0.2450
W2R1	2.97	-26759	-26756	0.0111
W2R2	6.32	-26611	-26605	0.0238
W2R3	17.68	-26645	-26627	0.0664
W3R1	2.13	-30096	-30094	0.0071
W3R2	3.22	-29936	-29933	0.0108
W3R3	12.21	-29901	-29889	0.0409

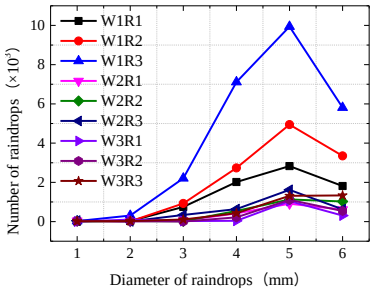

(a) Number of raindrops

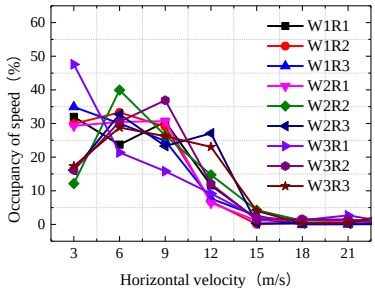

(b) Occupancy of velocity

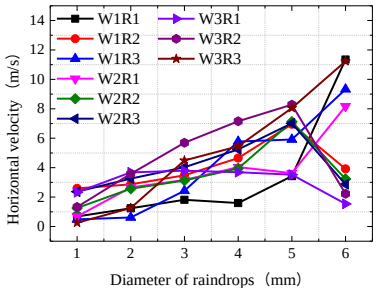

(c) Horizontal terminal velocity of raindrops

Fig. 10 Distribution curves of number and terminal velocity of raindrops with different diameters under different working conditions

5.3 Analysis of equivalent internal pressure coefficient

Rain loads on the internal surface of the cooling tower are calculated using formula (12) under 9 working conditions. The ratio of total raindrop load to total wind load is estimated as shown in Table 1. It can be seen that the rain load acting on the internal surface is very small as compared with the wind force, the maximum being only 0.245% of total wind and rain loads and occurring under working condition W1R3. The total rain load under different wind velocities increases with the rainfall intensity. The increase in wind velocity under constant rainfall intensity causes a significant reduction in rain load acting on the internal surface of the tower.

In order to compare the aerodynamic force distribution on the internal surface of the tower under the coupled wind and rain action for 9 working conditions, the equivalent internal pressure coefficient is defined as formula (17) ~ (19) below.

$$Cp_{ei} = Cp_{wi} + Cp_{ri} \tag{17}$$

$$Cp_{ri} = \frac{P_{ri}}{P_{wz_0}} \tag{18}$$

$$P_{ri} = \frac{F_{ri}}{S_i} \tag{19}$$

Where, Cp_{ei} is the equivalent internal pressure coefficient of the i monitoring point of the cooling tower under the combined action of wind and rain; Cp_{wi} is the wind induced internal pressure coefficient of the monitoring point; Cp_{ri} is the internal pressure coefficient of rain; P_{ri} is the pressure induced by rain; P_{wz0} is the pressure induced by wind at the reference height, the reference height in this paper is taken as the top 189m of the tower; F_{ri} is the wind load; S_i is the calculation area.

Circumferential equivalent internal pressure coefficients at four representative cross sections (i.e., middle of conical section, junction between straight and conical sections, middle of straight section and upper part of straight section) are compared under 9 working conditions, as shown in Fig. 11. It can be seen that

(1) Equivalent internal pressure coefficients differ slightly under each working condition when considering two-way coupling between wind and rain. There exists great difference in the distribution curves over cross sections at different heights. The curves are basically enveloped by those under working condition W3R3 and W1R3. The maximum difference in internal pressure coefficient is as large as 14.68% in some positions, occurring in the middle of the conical section under the working condition W3R1;

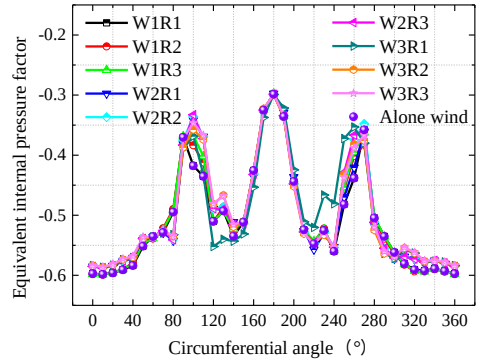

(a) Middle of conical section

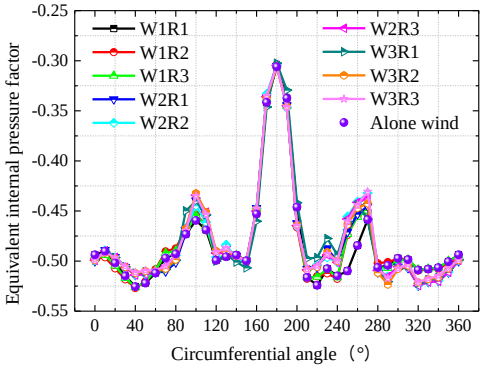

(b) Junction between straight and conical sections

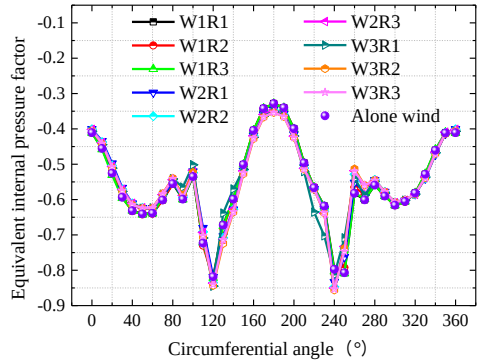

(c) Middle of straight section

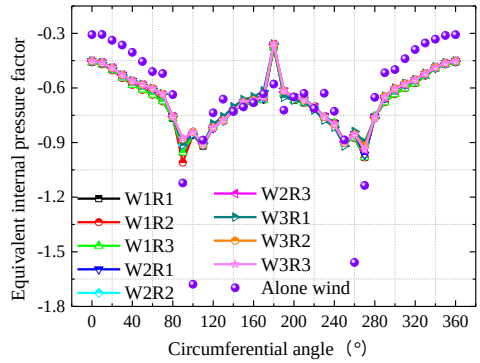

(d) Upper part of straight section

Fig. 11 Comparison of circumferential equivalent internal pressure coefficient over representative cross-sections of the cooling tower

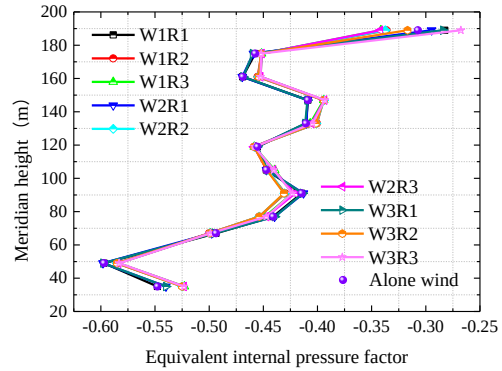

(a) 0°

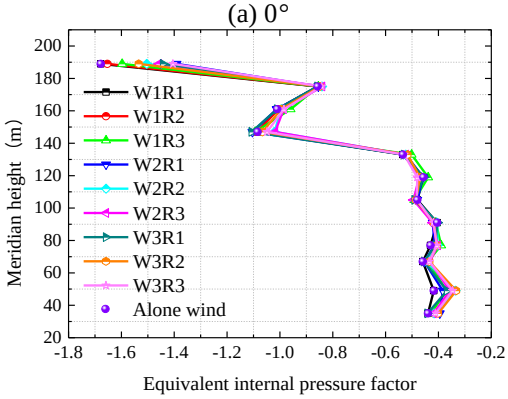

(b) 100°

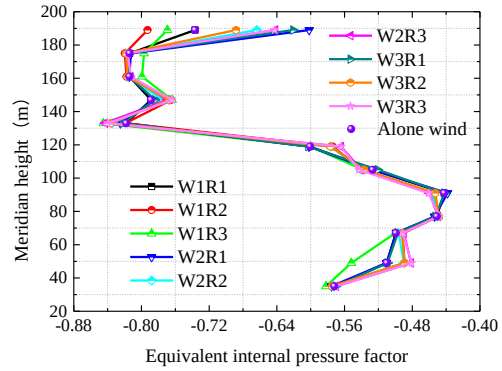

(c) 120°

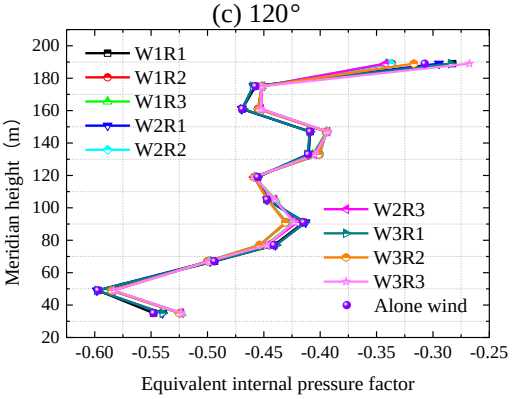

(d) 180°

Fig. 12 Comparison of meridional equivalent internal pressure coefficients under 9 working conditions

(2) Minimum equivalent internal pressure coefficients all occur in the leeward regions under different working conditions. The lower part of the cooling tower is mainly affected by the airflow passing through the shutters and impacting the internal wall surface of the tower; the upper part is related to the raindrops impacting the internal surface of the tower in the leeward region. The former has a greater influence on the internal pressure coefficient than the latter;

(3) The maximum equivalent internal pressure coefficient in the middle of the conical section occurs at the angle of 0°. As the height increases, the angles corresponding to the peak become 40°and 120°. For the upper part of the cylindrical section, the peak occurs at the angle of 90°in the center of cross-wind region, and the equivalent internal pressure coefficient of the cross-wind surface is significantly reduced by the rain load.

Four representative meridian lines (0°, 100°, 120° and 180°) are chosen to compare the equivalent internal pressure coefficients under 9 working conditions, as shown in Fig. 12. It can be seen that the distribution of meridional internal pressure coefficient differs greatly under different angles. The equivalent internal pressure coefficient at the angle of 100°has a larger value scope than at other meridional angles. Except for 0°, equivalent internal pressure coefficients at other angles basically increase with meridional height. A turning point occurs in the distribution of internal pressure coefficient at some heights due to the joint action of wind and rain. Unstable airflow at the air outlet causes an abrupt change in equivalent internal pressure coefficient at the tower top. However, the variation pattern is generally consistent under the same meridional angle between different working conditions, and the values are discretely distributed.

6. Influence of ventilation rate of shutters

Ventilation rate of shutters has a significant impact on the airflow and raindrop movements inside the cooling tower. The influence of ventilation rate on internal pressure of cooling tower is discussed under the most unfavorable working condition, i.e., working condition 3, which is the combination of wind velocity 20 m/s+rainfall intensity 200mm/h. The ventilation rate of shutters around the cooling tower is related to the construction stage and operational status (Ke *et al.* 2015). Four ventilation rates are considered: (1) construction stage: ventilation rate of 100%; (2) operational stage: ventilation rate of 15% and 30% under the design wind speed; (3) operational stage: ventilation rate of 0% when the shutters are completely closed during winter to prevent freezing.

The four ventilation rates (0%, 15%, 30% and 100%) correspond to working condition A, B, C and D, respectively. The computational model is shown in Fig. 13.

6.1 Influence of ventilation rate on wind field

Figs. 14 and 15 are the 3D wind velocity streamlines and distribution of turbulence kinetic energy under the four working conditions before considering the effect of raindrops. Comparison indicates that

(1) Part of the airflow separates and moves towards the two sides in front of the anterior margin of the cooling tower. The remaining part of the airflow ascends along the windward region of the structure and enters the tower from the tower top. The shutters are closed under working condition A, and airflow cannot move out from the bottom, therefore accumulating in the lower part of the tower. The airflow moves along the inner wall surface, colliding with the inner wall surface while ascending. The movement speed of the airflow increases suddenly at the junction between the straight and conical sections. The airflow stabilizes further upwards until it moves out from the air outlet.

(2) As the ventilation rate increases, an unobstructed wind channel is formed inside the cooling tower. The airflow accumulates less intensively, and the flow lines become sparse. There is a greater number of airflow entering the tower via the air inlet under complete ventilation. When this part of airflow collides with the airflow entering from the tower top, the flow lines become denser in the middle of the tower.

(3) Turbulence kinetic energy is directly proportional to the density of flow lines. It is greater at the tower top and first decreases and then increases with the increase of ventilation rate. The turbulence kinetic energy is lower at the air outlet under working condition C, while greater energy is distributed over the inner wall surface in the leeward region. The turbulence kinetic energy at the tower bottom is the smallest under working condition A, while it is the highest under working condition B, followed by working condition C and D successively.

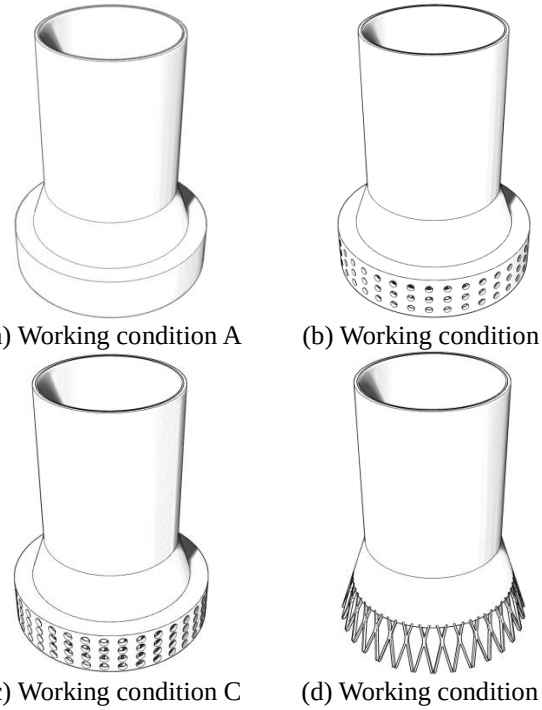

(a) Working condition A (b) Working condition B

(c) Working condition C (d) Working condition D

Fig. 13 Computational model under four ventilation rates

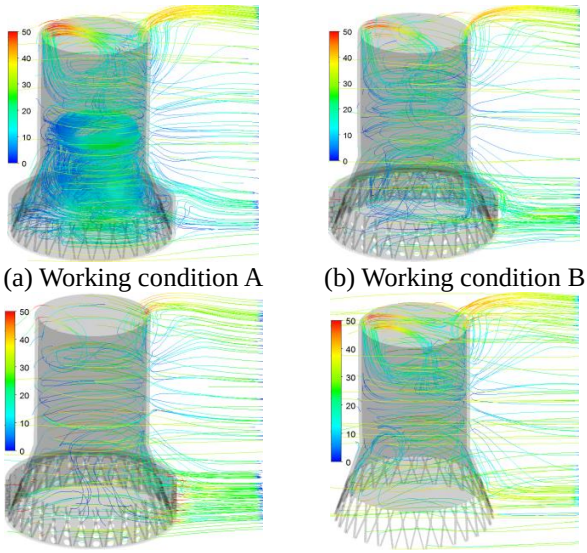

(a) Working condition A (b) Working condition B

(c) Working condition C (d) Working condition D

Fig. 14 3D Wind velocity streamlines under four ventilation rates

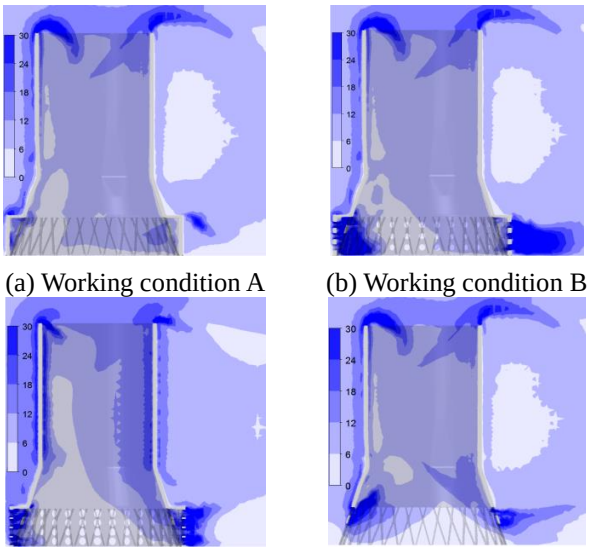

(a) Working condition A (b) Working condition B

(c) Working condition C (d) Working condition D

Fig. 15 Turbulence kinetic energy under four ventilation rates

6.2 Influence of ventilation rate on rain field

Fig. 16 shows the raindrop trajectories in the coupled wind and rain fields under the four working conditions. It can be seen that a large number of raindrops separate and move towards the two sides of the tower along the wall surface under the action of wind. Only a small portion of raindrops enter the tower. As the ventilation rate increases, the raindrop velocity increases in the crosswind region of the tower. Raindrops in the lower part of the tower enter the tower via the shutters, and then flow out of the tower without staying inside because of the wind. This phenomenon is even more significant under the ventilation rate of 100%.

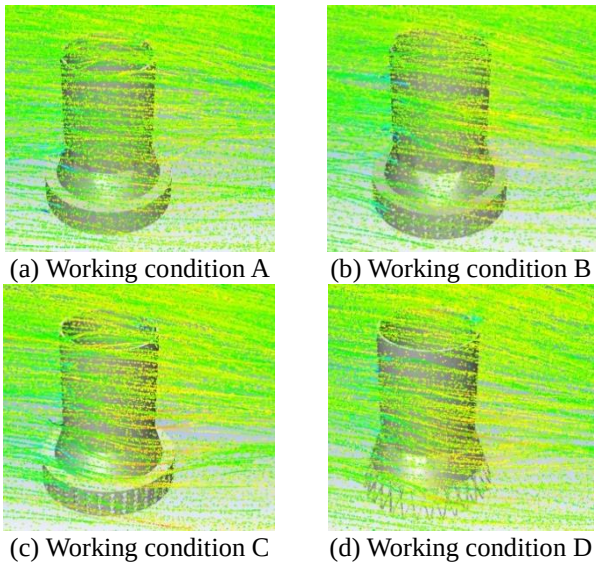

(a) Working condition A (b) Working condition B

(c) Working condition C (d) Working condition D

Fig. 16 Raindrop trajectories in the coupled wind and rain fields under four ventilation rates

Fig. 17 shows the 3D distribution of raindrops over the internal surface of cooling tower under the four working conditions. It can be seen that

(1) The volume of raindrops accumulating on the internal surface first decreases and then increases as the ventilation rate increases. Under the four working conditions, the raindrops are mainly found on the internal surface in the upper leeward regions, where the raindrops collide with the internal wall surface. The increase of ventilation rate makes the vortex movement more intensive inside the tower. The areas of internal wall surface impacted by the raindrops expand along the circumferential and meridional directions as the ventilation rate increases.

(2) Airflow enters the tower via the shutters and air outlet. During this process, the airflow moves at an increasing velocity and forms an intact vortex inside the tower. Some of the raindrops falling inside the tower change the trajectories before hitting the internal wall surface due to the action of vortex. As a result, the raindrops are scatteredly distributed in the windward and crosswind regions and the middle and lower parts of the tower body.

Fig. 18 is the comparison of number, impact velocity and occupancy of velocity of raindrops with different diameters under the four working conditions. It can be seen that

(1) The diameters of raindrops captured by the internal wall surface under different ventilation rates vary from 3 to 6mm, and raindrops with a diameter of 5mm account for the largest proportion. This is because the velocity of smaller raindrops increases more quickly under the same wind force. The raindrops already slide over the tower top and move towards the wake zone in the horizontal direction before entering the tower in the straight direction.

(2) The largest number of raindrops are accumulated under the working condition A. The occupancy of raindrops with varying diameters is the highest among the four working conditions. The number of smaller raindrops accumulating under the working condition B is higher than

under working condition A and C. Moreover, the number of raindrops with a diameter of 5 mm increases suddenly under the working condition 1.

(3) The velocity of raindrops impacting the internal surface ranges from 3 to 12 ms. The occupancy of impact velocity of 3 m/s is the highest under each working condition, with the maximum reaching 64.28%. The mean horizontal velocity of raindrops with varying diameter is far blow the baseline wind velocity (20 m/s).

6.3 Influence of ventilation rate on equivalent internal pressure

Rain loads on the internal wall surface of the tower are calculated under four working conditions, and the ratio to total loads is estimated, as shown in Table 5. It can be seen that the rain load on the internal wall surface is extremely small compared with wind force, the maximum only accounting for 0.6536%, which occurs under working condition A. The direction of the load imposed by raindrops is contrary to the direction of wind load, which partially counteracts the unfavorable impact of wind load on structure. The overall rain load is the largest when the ventilation rate is 0%. At other ventilation rates, the rain load dramatically decreases by 80%, and the load values are similar under different ventilation rates.

Circumferential equivalent internal pressure coefficients are compared over four representative cross sections, namely, i.e., middle of conical section, junction between straight and conical sections, middle of straight section and upper part of straight section. It can be seen from Fig. 19 that

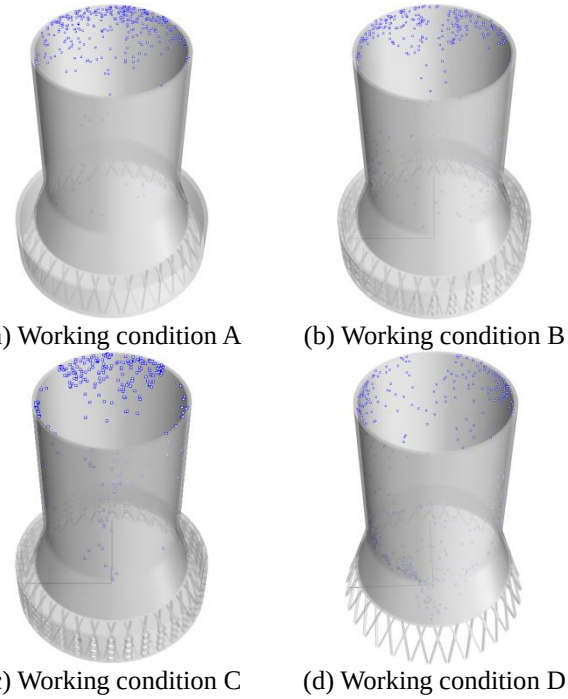

(a) Working condition A (b) Working condition B

(c) Working condition C (d) Working condition D

Fig. 17 3D distribution of raindrops over the internal wall surface of the tower under four ventilation rates

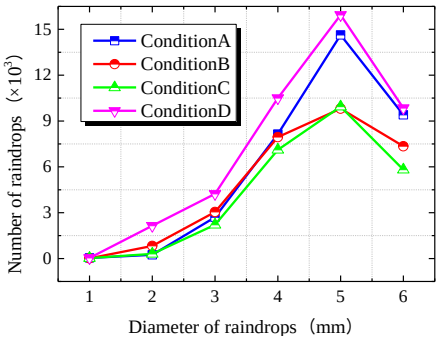

(a) Number of raindrops

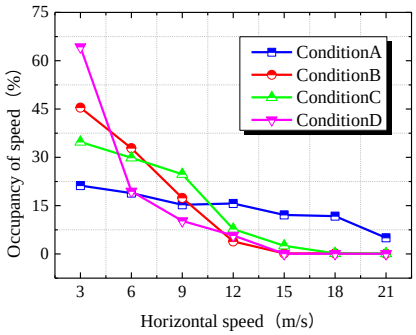

(b) Occupancy of velocity

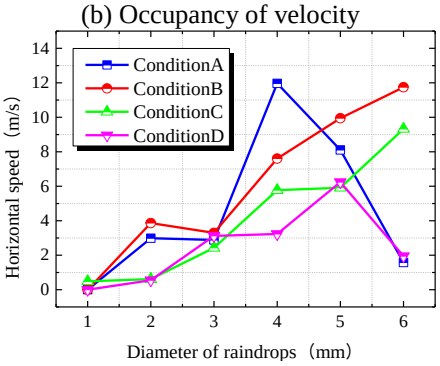

(c) Horizontal terminal velocity

Fig. 18 Number of raindrops with different diameter and horizontal terminal velocity of raindrops under four ventilation rates

(1) Ventilation rate has a significant influence on equivalent internal pressure coefficient on the internal wall surface. However, the distribution of circumferential internal pressure coefficient varies significantly over different cross sections. All distribution patterns are symmetrical around the wind axis. The absolute values of equivalent internal pressure coefficient in the leeward regions are smaller compared with other regions of the tower. The equivalent internal pressure coefficients vary from -1.2 to -0.2 under different working conditions.

(2) The equivalent internal pressure coefficients in the middle of the conical section and at the junction between the straight and conical sections are the highest under working condition A, followed by working condition B and C successively. The coefficient values are greatly influence by the strong airflow near the air inlet. The circumferential internal pressure coefficient under working condition D fluctuates violently, and the values are distributed over a large span.

Table 5 Comparison of wind and rain loads on the internal wall surface under different ventilation rates

Working condition	Overall rain load (kN)	Overall wind load (kN)	Total and rain loads (kN)	Ratio of rain load to total load (%)
A	157.19	-24206	-24049	0.6536
B	31.61	-18273	-18241	0.1733
C	40.93	-16744	-16703	0.2450
D	38.02	-16804	-16766	0.2268

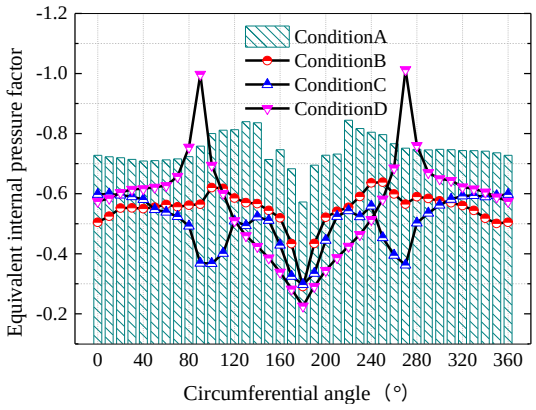

(a) Middle of conical section

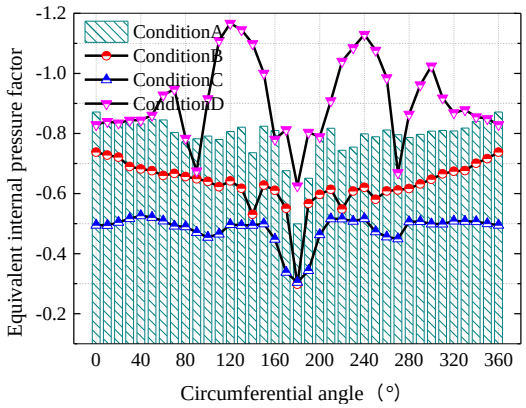

(b) Junction between straight and conical sections

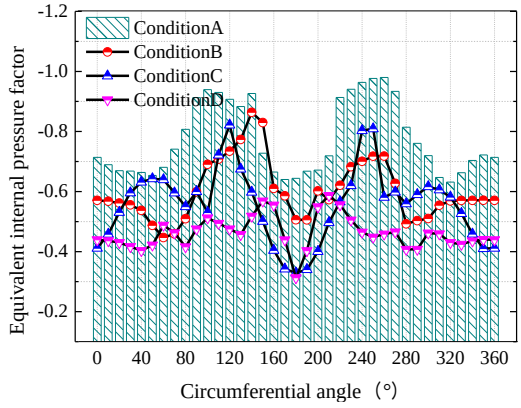

(c) Middle of straight section

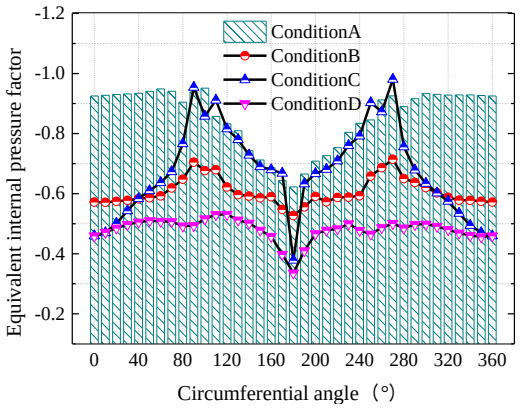

(d) Upper part of straight section.

Fig. 19 Comparison of circumferential equivalent internal pressure coefficients over representative cross sections under four ventilation rates

(3) The equivalent internal pressure coefficients in the middle and upper parts of the straight section are less affected by airflow at the air inlet. The coefficient values are the highest under working condition A, followed by working condition B and D, respectively. The changes of coefficient values are the most significant under working condition C.

Equivalent internal pressure coefficients are compared between four representative meridian lines (0°, 100°, 120° and 180°) under four ventilation rates, It can be seen from Fig. 20 that the meridional internal pressure coefficients vary significantly under different working conditions. When the ventilation rate is 100%, more air enters the tower and makes complex movements. Energy is concentrated at the junction between the conical and straight sections because of Bernoulli effect, where the internal pressure coefficient increases dramatically. In contrast, the internal pressure coefficient varies less violently in the straight section as the cross-sectional area is constant. At the tower top, the internal pressure coefficient shows large variation due to the joint action of raindrop impact and unstable airflow at the air outlet.

Based on the above analysis, the tower body is divided into four regions along the circumferential and meridional directions, respectively. Values of equivalent internal pressure coefficients are given for each region under different ventilation rates, as shown in Fig. 21. Thus the values of equivalent internal pressure coefficients can be

Continued-

directly used for different regions of the cooling tower during structural design.

Comparison would reveal that the equivalent internal pressure coefficients at the junction between the straight and conical sections first increases, then decreases and then increases again as the ventilation rate increases. The coefficient values are generally in a direct proportion to the ventilation rate within the range of height under consideration. The values within the interval of 140°-180° along the circumferential direction are the smallest compared with other intervals.

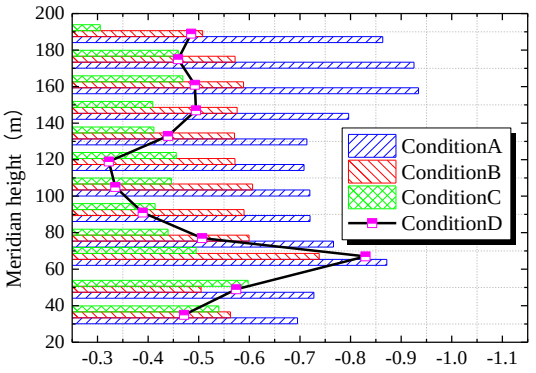

(a) 0°

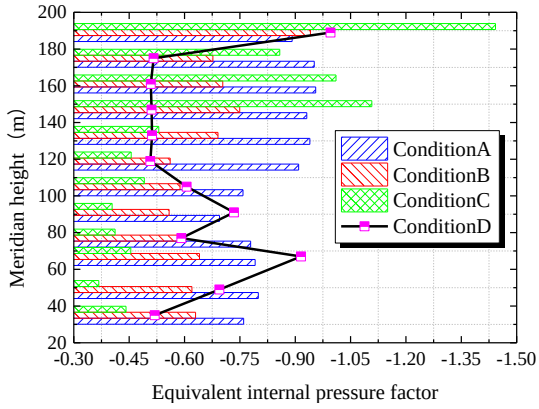

(b) 100°

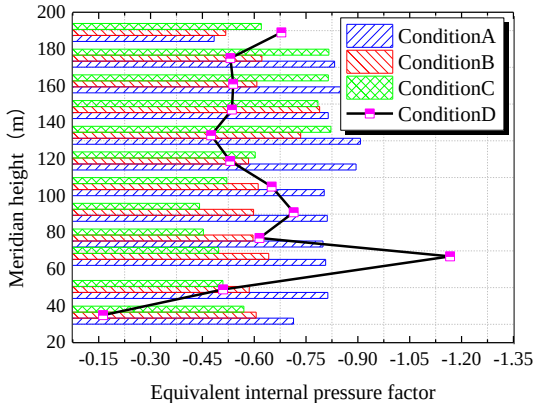

(c) 120°

Continued-

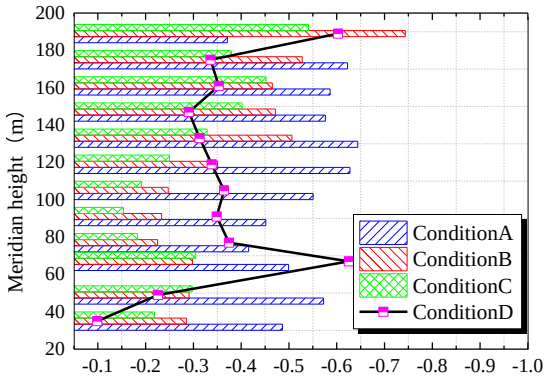

(d) 180°

Fig. 20 Comparison of equivalent internal pressure coefficients along representative meridian lines under four ventilation rates

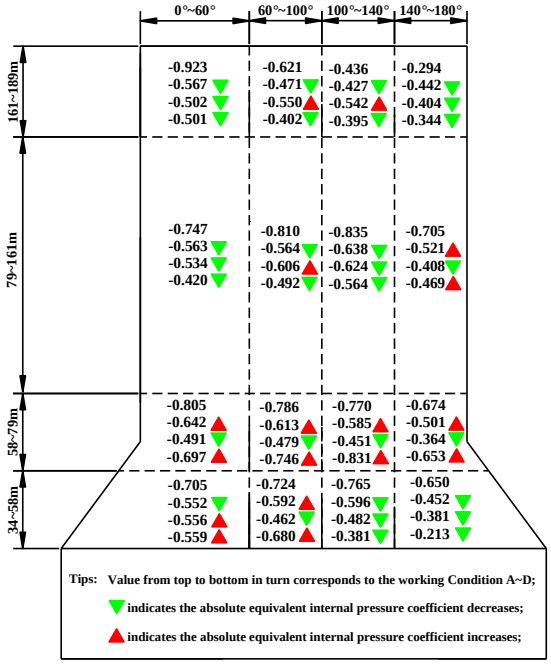

Fig. 21 Values of equivalent internal pressure coefficent for different regions of the tower under four ventilation rates

7. Conclusions

The aerodynamic performance and action mechanism of internal pressures in straight-cone steel cooling tower under two-way coupling between strong wind and heavy rain are discussed in this study. The wind field and rain field are simulated iteratively using continuous and discrete phase models, respectively. The following conclusions are drawn:

(1) Raindrops are subjected to greater horizontal force as wind velocity increases, and as a result, the raindrops move at an accelerating velocity. A large number of raindrops slide over the tower top and enter the wake zone because of the driving and enveloping effect of airflows in front of the tower and coming out of the tower via the air

outlet. Only a small portion of raindrops enter the tower and collide with the internal wall surface along with the airflows.

(2) The regions impacted by raindrops under different working conditions are generally the internal surfaces in leeward regions. The occupancy of diameter of 5mm and impact velocity of 3-12m/s is the highest. The number of raindrops accumulating on the internal surface decreases as the wind velocity increases. It first increases and then decreases as the ventilation rate of shutters increases. In addition, the areas impacted by raindrops gradually expand as the ventilation rate increases.

(3) The load imposed by raindrops on the internal surface accounts for an extremely small proportion of total load, the maximum being only 0.6536%, which occurs when the ventilation rate is zero under the wind velocity of 20m/s and rainfall intensity of 200 mm/h. On the whole, different combinations of wind velocity and rainfall intensity produce a small influence on the distribution of equivalent internal pressure coefficient.

(4) Different ventilation rate of shutters not only change the airflow movement inside the tower, but also the number and distribution of raindrops accumulating on the internal surface. The internal pressure is the highest at the ventilation rate of 0%, and circumferential and meridional changes are the most intensive at the ventilation rate of 100%.

(5) The equivalent internal pressure coefficient at the junction between the straight and conical sections first increases, then decreases and then increases again as the ventilation rate increases. The equivalent internal pressure coefficients in other regions are generally in a reverse proportion to the ventilation rate. The equivalent internal pressure coefficients are the smallest within the interval of 140° - 180° along the circumferential direction.

Acknowledgments

This project is jointly supported by National Natural Science Foundation (51761165022, 51208254), Jiangsu Province Natural Science Foundation (BK2012390), Jiangsu Qing Lan Project, Six talent peaks project in Jiangsu Province (JZ-026) and Postdoctoral Science Foundation (2013M530255; 1202006B), which are gratefully acknowledged.

References

Bennett, M., Kodakalla, V. and Gupta, V. (2011), "Vibration mitigation measures in cable stayed bridges", *J. Molecular Struct.* **996**(1-3), 64-68.

Blocken, B., Dezsö, G., Beeck, J.V. and Carmeliet, J. (2010), "Comparison of calculation models for wind-driven rain deposition on building facades", *Atmosp. Environ.*, **44**(14), 1714-1725.

Blocken, B. and Carmeliet, J. (2004), "A Review of Wind-Driven Rain Research in Building Science", *J. Wind Eng. Ind. Aerod.*, **92**, 1079-1130.

Blocken, B. and Carmeliet, J. (2002), "Spatial and temporal distribution of driving rain on alow-rise building", *Wind Struct.*, **5**(5), 441-462.

BS4485(Part 4) (1996), Code of practice for structural design and construction-water cooling tower. *London: British Standard Institution*.

Cheng, X.X., Zhao, L. and Ge, Y.J. (2013), "Multiple loading effects on wind-induced static performance of super-large cooling towers", *Int. J. Struct. Stab. Dynam.*, **13**(8).

DL/T 5339-2006 (2006), Code for hydraulic design of fossil fuel power plants. *The Ministry of Construction of China*, Beijing, China, 115-116. (in Chinese)

Dong, G.C., Zhang, J.R., Cai, C.S. and Han Y. (2016), "Study on internal surface pressure coefficient of super-large cooling tower with different internal main components", *Eng. Mech.*, **33**(4), 77-83. (in Chinese)

Douvi, E. and Margaris, D. (2012), "Aerodynamic performance investigation under the influence of heavy rain of a NACA 0012 airfoil for wind turbine applications", *Int. Rev. Mech. Eng.*, **6**(6).

Du, L.Y. and Ke, S.T. (2016), "Research on effect of internal pressures for super large cylinder-conic section steel cooling towers", *J. Central south University*, accepted, forthcoming. (in Chinese)

Fu, X., Li, H.N. and Li, G. (2016), "Fragility analysis and estimation of collapse status for transmission tower subjected to wind and rain loads", *Struct. Saf.*, **58**, 1-10.

GB50009-2012 (2012), Load code for the design of building structures. *The Ministry of Construction of China*, Beijing, China, 35-36. (in Chinese)

Goudarzi, M.A. and Sabbagh-Yazdi, S.R. (2011), "Effects of modeling strategy on computational wind pressure distribution around the cooling towers", *Wind Struct.*, **14**(1), 81-84.

Gunn, R. and Kinzer, G.D. (1949), "The terminal fall velocity for water droplets in stagnant air", *J. Atmos. Sci.*, **6**(4), 243-248.

Ke, S.T., Ge, Y.J., Zhao, L. and Tamura, Y. (2015), "Stability and reinforcement analysis of super large exhaust cooling towers based on a wind tunnel test", *J. Struct. Eng.*, **141**(12), 04015066.

Ke, S.T., Liang, J., Zhao, L. and Ge, Y.J. (2015), "Influence of ventilation rate on the aerodynamic interference for two IDCTs by CFD", *Wind Struct.*, **20**(3), 449-468.

Li, L.X., Kareem, A., Xiao, Y.Q. and Zhou, C. (2015), "A comparative study of field measurements of the turbulence characteristics of typhoon and hurricane winds", *J. Wind Eng. Ind. Aerod.*, **140**, 49-66.

Liu, S., Huang, S.H. and Li, Q.S. (2017), "3D numerical simulation of wind-driven rain on bridge deck sections based on eulerian multiphase model", *Eng. Mech.*, **34**(4), 63-71. (in Chinese)

Marshall, J.S. and Palmer, W.M. (1948), "The distribution of raindrops with size", *J. Meteorology*, **5**, 165-166.

Mcfarquhar, G.M. and List, R. (2010), "The raindrop mean free path and collision rate dependence on rainrate for three-peak equilibrium and marshall-palmer distributions", *J. Atmos. Sci.*, **48**(48), 1999-2004.

Rigby, E.C., Marshall, J.S. and Hitschfeld, W. (2010), "The development of the size distribution of raindrops during their fall", *J. Atmo. Sci.*, **11**(5), 362-372.

VGB-R610Ue (2005), VGB-Guideline: structural design of cooling tower-technical guideline for the structural design, computation and execution of cooling towers. *Essen: BTR Bautechnik Bei Kuhlturmen*.

Wang, L.Y. and Xu, Y.L. (2010), "Active stiffness control of wind-rain-induced vibration of prototype stay cable", *Int. J. Numer. Method. Eng.*, **74**(1), 80-100.

Wang, Z., Zhao, Y., Li, F. and Jiang, J. (2013), "Extreme dynamic responses of mw-level wind turbine tower in the strong typhoon considering wind-rain loads", *Math. Probl. Eng.*, **3**, 133-174.

Xin, D., Li, H., Wang, L. and Ou, J. (2012), "Experimental study on static characteristics of the bridge deck section under simultaneous actions of wind and rain", *J. Wind Eng. Ind. Aerod.*, **s**(107-108), 17-27.

Zhang, Q.C., Li, W.Y. and Wang, W. (2010), "Static bifurcation of rain-wind-induced vibration of stay cable", *Acta Physica Sinica*, **59**(2), 729-734.

CC